Chemical Science

EDGE ARTICLE

View Article Online
View Journal | View Issue

Cite this: *Chem. Sci.*, 2017, **8**, 325

On the molecular mechanisms for the H_2/CO_2 separation performance of zeolite imidazolate framework two-layered membranes†

Fernando Cacho-Bailo,[a] Ismael Matito-Martos,[b] Julio Perez-Carbajo,[b] Miren Etxeberría-Benavides,[c] Oğuz Karvan,[c] Víctor Sebastián,[ad] Sofía Calero,*[b] Carlos Téllez[a] and Joaquín Coronas*[a]

Received 3rd June 2016
Accepted 6th August 2016

DOI: 10.1039/c6sc02411d

www.rsc.org/chemicalscience

Double-layered zeolitic imidazolate framework (ZIF) membranes were fabricated inside polyimide P84 hollow fibers by a step-synthesis conducted by microfluidic technology and applied to pre-combustion gas separation. Our hypothesis, based on the information provided by a combination of molecular simulation and experiments, is that a CO_2 adsorption reduction on the surface of the ZIF-9 would enhance the molecular sieving effect of this ZIF-9 layer and therefore the selectivity in the H_2/CO_2 mixture separation of the entire membrane. This reduction would be achieved by means of a less-CO_2-adsorptive methylimidazolate-based ZIF-67 or ZIF-8 layer coating the ZIF-9. ZIF-8/ZIF-9 and ZIF-67/ZIF-9 double-layered membranes were prepared and characterized by XRD, FTIR, SEM, FIB, TEM and EDS. This unprecedented strategy led to a H_2/CO_2 separation selectivity of 9.6 together with a 250 GPU H_2 permeance at 150 °C, showing a significant improvement with respect to the pure ZIF-9 membrane. Double-layered membranes also showed higher apparent CO_2 activation energies than single-layered membranes, attributable to a diminished adsorption.

1. Introduction

Carbon capture and storage (CSS) is a widespread strategy used to combat the increasing concentration of greenhouse effect gases in the atmosphere as well as global warming.[1] Almost 20 years after the signing of the Kyoto protocol, the United Nations agreement at the Paris Climate Conference in 2015 highlighted the importance of reducing CO_2 emissions from fossil fuel combustion.[2] It is clear that research & development efforts must focus on improving the technologies available for CO_2 separation. Membranes can provide an eco-friendly and low energy consumption alternative to traditional separation techniques.[3,4]

Highly pressurized pre-combustion streams have important advantages over post-combustion in carbon capture with membranes. Therefore the H_2/CO_2 gas mixture separation is crucially important in CSS.[2,3] Metal–organic framework (MOF)-based membranes have been applied to the treatment of post-combustion gas mixtures (CO_2/N_2) with promising results, owing to an enhanced adsorption–diffusion mechanism favouring CO_2 through the membrane.[5] Supported CAU-1 by Yin *et al.*,[6] ZIF-7 in our previous work[7] and ZIF-90 by Brown *et al.*[8] led to 22.8, 13.6 and 3.5 CO_2/N_2 separation selectivities, respectively. Liu *et al.* grew a CO_2-selective preferentially oriented ZIF-69 membrane (CO_2/N_2 selectivity of 6.3),[9] while Tzialla *et al.* subsequently functionalized this ZIF-69 with a cation based ionic liquid.[10] Zhao *et al.* achieved a CO_2/N_2 selectivity of 60 at 298 K with a 14 μm thick MOF-5 membrane and studied the influence of the feed pressure and composition.[11] In addition, mixed matrix membranes (MMMs) using MOFs as fillers have also been used for the separation of this mixture.[12–15] Adatoz *et al.* summarized the computational and experimental studies on both thin-film and MOF composite membranes and addressed their challenges in practical gas separations.[16]

However, the kinetic diameter of H_2 (2.9 Å) is noticeably smaller than that of N_2 (3.6 Å) and even CO_2 (3.3 Å). In consequence, H_2/CO_2 separation requires a MOF-material with a very restricted pore and distinct adsorptive properties. Crystalline nanoporous structures of zeolitic imidazolate frameworks (ZIFs) with pore diameters between 3 and 5 Å are ideal for use as molecular sieves in the separation of gas molecules with small kinetic diameters.[17] ZIF-7 and ZIF-9, both based on the voluminous benzimidazolate ligand and having a sod-structure with

[a]*Chemical and Environmental Engineering Department and Instituto de Nanociencia de Aragón (INA), Universidad de Zaragoza, 50018 Zaragoza, Spain. E-mail: coronas@unizar.es; Tel: +34 976762471*

[b]*Faculty of Experimental Sciences, University Pablo de Olavide, 41013 Sevilla, Spain. E-mail: scalero@upo.es; Tel: +34 954978312*

[c]*Tecnalia Research and Innovation, Energy and Environmental Division, 20009 Donostia-San Sebastian, Spain*

[d]*CIBER de Bioingeniería, Biomateriales y Nanomedicina, CIBER-BBN, 50018 Zaragoza, Spain*

† Electronic supplementary information (ESI) available. See DOI: 10.1039/c6sc02411d

very restricted limiting pore diameters of 3.0 Å,[18–20] would be appropriate to separate H_2 from the H_2/CO_2 mixture. However, the similar sizes of the molecules (2.9 for H_2 and 3.3 Å for CO_2) and the preferential adsorption affinity of CO_2 on ZIFs, especially in those formed with ligands containing nucleophile groups due to the high quadrapole moment of the molecule, would seem to lead to weak H_2/CO_2 separation selectivities at low temperatures.[21–26]

The flexibility of the metal–ligand bond forming ZIF structures provides effective pore limiting diameters noticeably higher than those predicted for these materials.[27–29] Unlike rigid zeolites, inorganic–organic ZIFs 'open their gates' and can therefore host molecules larger than expected.[30] For instance, Gücüyener *et al.* performed the uptake and release of light hydrocarbons in ZIF-7,[31] whereas Liédana *et al.* studied the encapsulation of bulky caffeine in ZIF-8.[32] Kolokolov *et al.* described the ZIF-8 ligand mobility opening the structure cavities like a saloon door.[33] Some recent molecular simulation studies already include flexible bonding conditions that allow the prediction of worse gas separation efficiencies than those expected from simulations when working with ZIFs.[34,35] Zhao *et al.* observed the influence of the CO_2 pressure on its adsorption on benzimidazole ZIF-7 and ZIF-9 and their phase transition response.[36–38]

To improve these pre-combustion stream separation selectivities, higher working temperatures would provide greater H_2 permeation flows while simultaneously decreasing CO_2 surface adsorption. Caro *et al.* have reported on the use of several ZIF-material supported membranes made of ZIF-95,[39] functionalized ZIF-90,[40] ZIF-7 (ref. 19) and ZIF-100 (ref. 41) for H_2/CO_2 separation at working temperatures up to 325 °C. At the same time, some MOFs have revealed a high CO_2 adsorption capacity and therefore a useful application in gas separation by membranes even at room temperature,[42] as shown in several works by Li *et al.* with H_2/CO_2 ideal separation factors of 21 and 32 for HKUST-1 (ref. 43) and NH_2-MIL-53,[44] respectively. However, Peng *et al.* reported an exceptionally high H_2/CO_2 separation selectivity (291) by using an exfoliated ZIF-7 as a membrane building block.[45]

Fig. 1 depicts our approach for a better pre-combustion H_2/CO_2 separation based on the creation of a double-layered ZIF membrane, an idea already implemented with zeolites (*e.g.* silicalite-1/ZSM-5,[46] ZSM-5/mordenite,[47] and LTA/FAU types[48]). This combines a positive molecular sieving effect (due to the ZIF-9 layer with highly restricted pores of 3.0 Å) with a low CO_2 surface adsorption (because either ZIF-8 or ZIF-67 are made with a less CO_2 adsorptive methylimidazolate ligand and with pores of 3.4 Å), taking advantage of a step-synthesis by microfluidics.[7,49] A synergistic effect was expected: ZIF-8 on the surface would decrease the preferential CO_2 adsorption, while ZIF-9 would increase the sieving effect, thus enhancing the H_2 separation. This hypothesis was previously validated by molecular simulations and then experimentally using co-polyimide supported double-layered hollow fiber membranes. The different metallic character of the ZIF materials chosen (Zn in ZIF-8, and Co in ZIF-67 and ZIF-9) facilitated the characterization of the fabricated membranes.

2. Experimental and simulation

2.1. Membrane syntheses

Double-layered ZIF-8/ZIF-9@P84 and ZIF-67/ZIF-9@P84 membranes were synthesized with our microfluidic system, used in previous works to fabricate MOF membranes inside polymeric hollow fiber (HF) supports.[7,49,50] Zinc nitrate hexahydrate ($Zn(NO_3)_2 \cdot 6H_2O$, 98%, Sigma-Aldrich), cobalt nitrate hexahydrate ($Co(NO_3)_2 \cdot 6H_2O$, 98%, Sigma-Aldrich), cobalt acetate tetrahydrate ($Co(CH_3COO)_2 \cdot 4H_2O$, reagent grade, Sigma-Aldrich), ammonium hydroxide solution (NH_4OH, 28–30% NH_3 basis, Sigma-Aldrich), sodium formate (NaCOOH, 99%, Sigma-Aldrich), benzimidazole (bIm, 98%, Sigma-Aldrich) and 2-methylimidazole (mIm, 99%, Sigma-Aldrich) were used as received without further purification. ZIF layers were crystallized stepwise on the inner surface of a P84 (BTDA-TDI/MDI, 3,3′,4,4′-benzophenone tetracarboxylic dianhydride, 80% methylphenylene-diamine + 20% methylene diamine) co-polyimide hollow fiber of 333 μm OD and 222 μm ID. The procedure for the hollow fiber support fabrication can be found elsewhere.[49,50]

First, the inside of the P84 support was thoroughly washed with deionized water. Then a ZIF-9 ($Co(bIm)_2$) layer was crystallized using liquid phase epitaxial (LPE) synthesis. Solution A (0.2 mol L^{-1} cobalt acetate and 0.4 mol L^{-1} NH_4OH in absolute

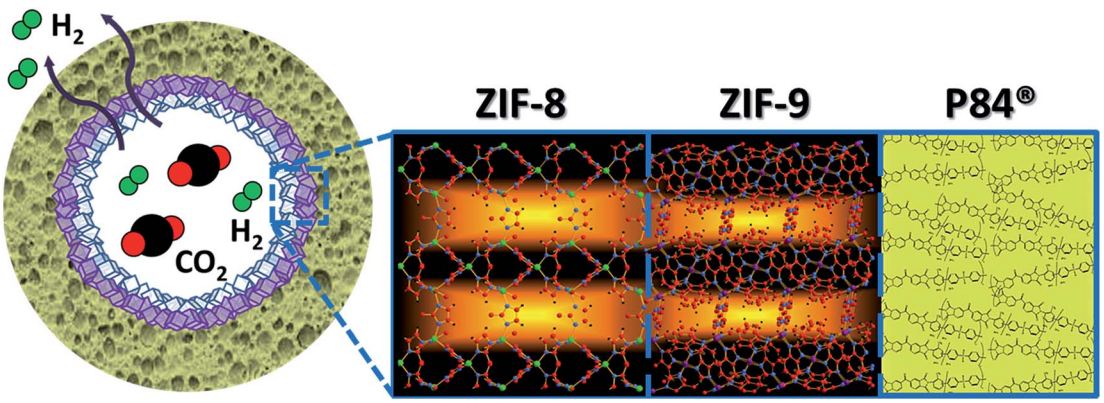

Fig. 1 Scheme of the double-layered ZIF-8/ZIF-9 membrane inside a polymeric (P84) hollow fiber for H_2/CO_2 separation.

ethanol) and solution B (0.2 mol L^{-1} benzimidazole in absolute ethanol) were pumped from 20 mL syringes inside the hollow fiber support alternatively in 4 runs of 2 mL each (totalling 8 mL A + B solution) at a 50 μL min^{-1} flow rate. Absolute ethanol was injected between each run (0.1 mL at the same flow rate) to prevent clogging, and also at the beginning and end to wet and wash the membrane (2 mL each).

ZIF-8 ($Zn(mIm)_2$) layer was crystallized immediately afterwards. Solution C (0.1 mol L^{-1} zinc nitrate in methanol) and solution D (0.3 mol L^{-1} 2-methylimidazole and 0.3 mol L^{-1} NaCOOH in methanol) were injected together at a rate of 50 μL min^{-1} totalling 6 mL C + D solution. Finally, the inside of the membrane was washed with methanol at 50 mL min^{-1} and dried at room temperature for at least 24 h. ZIF-67 ($Co(mIm)_2$) was obtained when cobalt nitrate was used instead of zinc salt.

In the same manner, membranes with a single MOF layer (ZIF-9 and ZIF-8) were fabricated following the corresponding individual procedure described above. Powders collected for characterization in every synthesis were separated by centrifugation (10 000 rpm for 10 min) and washed appropriately.

2.2. Characterization and permeation tests

XRD (X-ray diffraction) spectra of the ZIF powdered materials were obtained using a D-Max Rigaku X-ray diffractometer (40 kV, 80 mA) with a Cu Kα ($\lambda = 1.542$ Å) rotating anode from 4 to 36° (2θ) with a 0.025° s^{-1} step. An XRD spectrum of the double-layered ZIF HF membranes cut in pieces was obtained with a 0.002° s^{-1} step and a scan time of 500 s per step. FTIR (Fourier Transform Infrared Spectroscopy) spectra were obtained using a Bruker Vertex 70, accumulating 20 scans from 4000 to 400 cm^{-1} with a 4 cm^{-1} resolution. CO_2 isotherms of the cobalt–ZIF powdered materials (ZIF-9 and ZIF-67) were obtained at 25 °C using a Micromeritics ASAP 2020. Samples were previously degassed at 200 °C for 8 h. Cross-section SEM (scanning electron microscopy) images were obtained using a FEI™Nova200 at 20 kV with a cryo-transfer chamber. The HF membrane sample was cooled in liquid N_2, cross-cut and Pt-sputtered inside the microscopy device. With the same device, a lamella was obtained from a ZIF-8/ZIF-9@P84 membrane by means of cryo-focused ion beam (FIB) equipment, using Ga atoms for the etching, to analyse the MOF–polymer interface by STEM. Metallic elemental analyses by EDS (energy dispersive spectroscopy) were carried out with an INCA PentaFET x3 (Oxford Instruments). The lamella, with a thickness of about 50 nm, was further examined by transmission electron microscopy (TEM, FEI™Tecnai G2 F30 microscope with a HAADF detector at 300 kV).

The gas permeation setup (Fig. S1 from the ESI†) for hollow fiber membranes is described in detail elsewhere.[7,49] Before the permeation tests, P84-supported membranes were *in situ* pre-treated at 175 °C for 24 h (with 6 h heating and cooling rates) in an H_2/CH_4/Ar atmosphere, to enhance MOF–polymer compatibility and therefore improve the membrane performance.[50] Then, an equimolar H_2/CO_2 gas mixture was fed inside the HF membrane at 10 cm^3 (STP) min^{-1}, while an Ar gas stream swept the permeate stream and provided the necessary driving force across the membrane, the total pressure drop being zero. The permeate composition was analyzed using a MicroGC Agilent 3000A gas chromatograph. Permeance values in mol m^{-2} s^{-1} Pa^{-1} were calculated using the log-mean partial pressure difference along the hollow fiber. Separation selectivities (α) were calculated as the ratio of permeances.[7] It is worth mentioning that ZIF membranes in this work have been under stream in the 35–175 °C range (including both pretreatment and separation operation) for at least 48 h and in some cases up to 120 h without evident loss of performance.

2.3. Simulation models and methods

RASPA code was used to carry out the simulations.[51] The adsorption isotherms were calculated using Monte Carlo simulations in the grand canonical ensemble. These simulations consisted of at least 2×10^5 equilibration cycles and 2×10^6 production cycles. Regrow, rotation, translation, insertion and deletion trial moves were randomly selected in each cycle. Simulations for ZIF-8 and ZIF-67 were performed with the same force fields and models used for the understanding of the gas-induced deformation of ZIF-8, providing good agreement between the experimental and simulation capacities.[52] For H_2 and CO_2, previously validated force fields were used,[53,54] with Lorentz–Berthelot mixing rules for the mixed Lennard-Jones parameters. Coulombic interactions were computed using the Ewald summation technique with a relative precision of 10^{-6}, and both electrostatic and Lennard-Jones cutoffs were fixed at 12 Å. Simulations for ZIF-9 were carried out using the crystallographic structure reported by Yaghi and coworkers.[55]

3. Results & discussion

Fig. 2 shows the experimental CO_2 adsorption isotherms at 25 °C of the ZIF-9 and ZIF-67 powders, collected during the membrane syntheses, and that of ZIF-8 from Zornoza *et al.*[56]

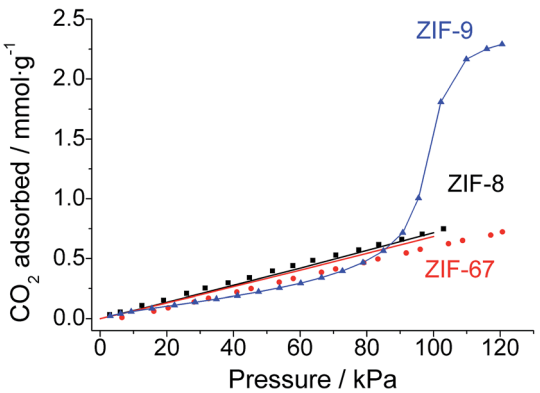

Fig. 2 Experimental CO_2 adsorption isotherms at 25 °C of the powdered cobalt-based materials ZIF-9 (blue triangles) and ZIF-67 (red circles), compared with the ZIF-8 CO_2 isotherm (black squares) reported by Zornoza *et al.*[56] Solid lines show simulated ZIF-8 (black) and ZIF-67 (red) isotherms with a good fit to the experimental data (filled symbols). The solid line in the ZIF-9 isotherm is a guide to the eye.

The Figure also includes the simulated isotherms calculated in this work for ZIF-67 and ZIF-8. CO_2 adsorption loading is about three times higher (2.3 mmol g^{-1}) in $Co(bIm)_2$ ZIF-9 than in mIm-based ZIF-67 and ZIF-8 (0.7 and 0.8 mmol g^{-1}, respectively), in agreement with previous experimental works[57–59] and with our simulations. These results represent the starting point for the double-layered membrane approach proposed here. The presence of ZIF-8 (or ZIF-67) material coating the ZIF-9 would diminish the CO_2 occupancy on the membrane surface, therefore favouring selective H_2 permeation.

The different adsorption capacities can be related to the ZIF composition. CO_2 molecule has an important quadrupole moment and is therefore attracted by highly charged polar groups such as hydroxyl or amine substituents. Likewise, the benzimidazolate ligand forming ZIF-9 contains benzene rings with a delocalized negative charge on which CO_2 acts as a Lewis acid and adsorbs preferentially. The absence of strong nucleophile groups in the methylimidazolate-based ZIFs (ZIF-67 and ZIF-8) justifies the low CO_2 adsorption observed.[60,61]

Molecular simulations give information about the transport mechanisms taking place in the membrane and anticipate the advantages of using double-layered membranes for the separation of H_2 and CO_2. Also the relevance of the sequence in the MOF growth chosen for the stepwise membrane synthesis (ZIF-8 or ZIF-67 material coating the ZIF-9 and in contact with the feed gas mixture) is evidenced. Based on the calculated adsorption isotherms in ZIF-8 and ZIF-67, the adsorption under the experimental conditions for equimolar mixtures of H_2 and CO_2 give rise to a permeate stream enriched in H_2, with a new mixture molar composition of 97/3 (H_2/CO_2). The advantage of this H_2-enriched mixture is twofold. Firstly, the large reduction of CO_2 in the flue gas exiting the mIm-MOF layer reduces the hydrogen–carbon dioxide competition when the mixture encounters the ZIF-9 material, thereby improving the sieving separation performance of this layer. Secondly, the lower CO_2 presence in the new flue gas mixture affects the pressure at which the gas enters the ZIF-9 layer. This second factor is particularly important for ZIF-9, since this structure acts as a valve that opens and closes for CO_2 as a function of pressure according to our simulations.

It is worth mentioning that, as recently pointed out,[36] ZIF-9 exhibits phase transitions upon loading that cannot yet be reproduced with molecular simulations. In fact, Fig. S2 of the ESI† shows that the calculated adsorption of CO_2 starts at much lower pressure values than those obtained experimentally. To the best of our knowledge, this is the first attempt to perform adsorption isotherms using molecular simulations in this particular structure. This indicates kinetic limitations that the Monte Carlo method cannot take into account. In particular, it seems like a plausible explanation that the adsorption of CO_2 in this structure is either hindered or triggered by the effect exerted by pressure and loading on the rotation of organic ligands. In any case, we still lack the methodology needed to reproduce the gate-opening phenomenon in the ZIF-9 structure. In spite of this serious computational limitation, we can still provide an interpretation of the molecular mechanisms involved in these systems from the combination of experimental isotherms and the simulations obtained from the crystallographic structure. Based on the simulations performed for ZIF-8 and ZIF-67 under these conditions (Fig. S3 and S4†) and considering the differences in pore size distributions calculated for the three structures (Fig. S5 and Table S1†), the pressure at which CO_2 would start entering the ZIF-9 structure for the new H_2-enriched mixture can be inferred to be at least 100 kPa. This pressure is more than one order of magnitude larger than that required for the gate-opening when working with pure CO_2.

We would like to emphasize the methodological difficulties in the development of force fields and methods to reproduce the adequate rotation of the organic ligands of ZIFs upon loading and diffusion. Indeed, these methods and force fields are still limited to ZIF-8. For this particular structure more than four years were needed, starting in 2011 with the first attempts to understand the adsorption isotherms of light gasses at low temperatures,[30,52] and ending in 2015 with the development of the fully flexible models and the complex specific methods required to understand the mechanisms involved in the gas diffusivity within the ZIF-8 pores.[34,62] In any event, the molecular simulations carried out justify the experimental implementation of our strategy based on double-layered ZIF membranes inside polymeric HF supports fabricated stepwise by microfluidics.

The synthesized ZIF-8/ZIF-9@P84 membrane was characterized in depth, as observed in Fig. 3. A continuous well-intergrown MOF layer was deposited on the inner surface of the co-polyimide P84 hollow fiber support, 2.0 ± 0.4 μm thick on average (Fig. 3a), showing a good adherence with the polymer with interpenetration of both phases. Since the two ZIF layers, as observed by SEM, do not appear to the naked eye to be separated, linear elemental analyses (EDS) were applied, taking advantage of the bimetallic character of the crystallized MOFs. Zinc and cobalt concentrations (coming from ZIF-8 and ZIF-9, respectively) are plotted in Fig. 3b with respect to the depth in the membrane, marked with a white line. ZIF-8 (Zn) was mostly found on the external side of the double-layered membrane, which is in contact with the feed gas mixture, and infiltrated to some depth indicating that a ZIF-8 layer had grown coating the initially prepared ZIF-9 membrane. ZIF-9 (Co) was also present and confined as an interphase between ZIF-8 and the polymer support. The interface between ZIF-8 and ZIF-9 may be a zone of metal and ligand exchange, displaying intermediate ZIF-8/ZIF-9 properties similarly to those ZIFs prepared by ligand exchange.[27,28,63] However, the detection of Zn close to the polymer support was very scarce, thus suggesting the presence of pure ZIF-9. In fact, some cobalt metal was also found about 1 μm inside the support pores, probably due to the liquid phase epitaxy (LPE) growing method[64] used for its crystallization, and accounting for some penetration of the ZIF synthesis into the hollow fiber pores. Fig. 3c–e show STEM-HAADF images at different magnifications focusing on the ZIF/polymer interphase. A thin (50 nm) lamella was obtained by cryo-FIB for this purpose. Areas with high brightness correspond to the location of the MOF material, since the HAADF detector is sensitive to the Z-contrast. Fig. 3f and g show the EDS mapping and the local spectra of the selected areas in Fig. 3e. Both

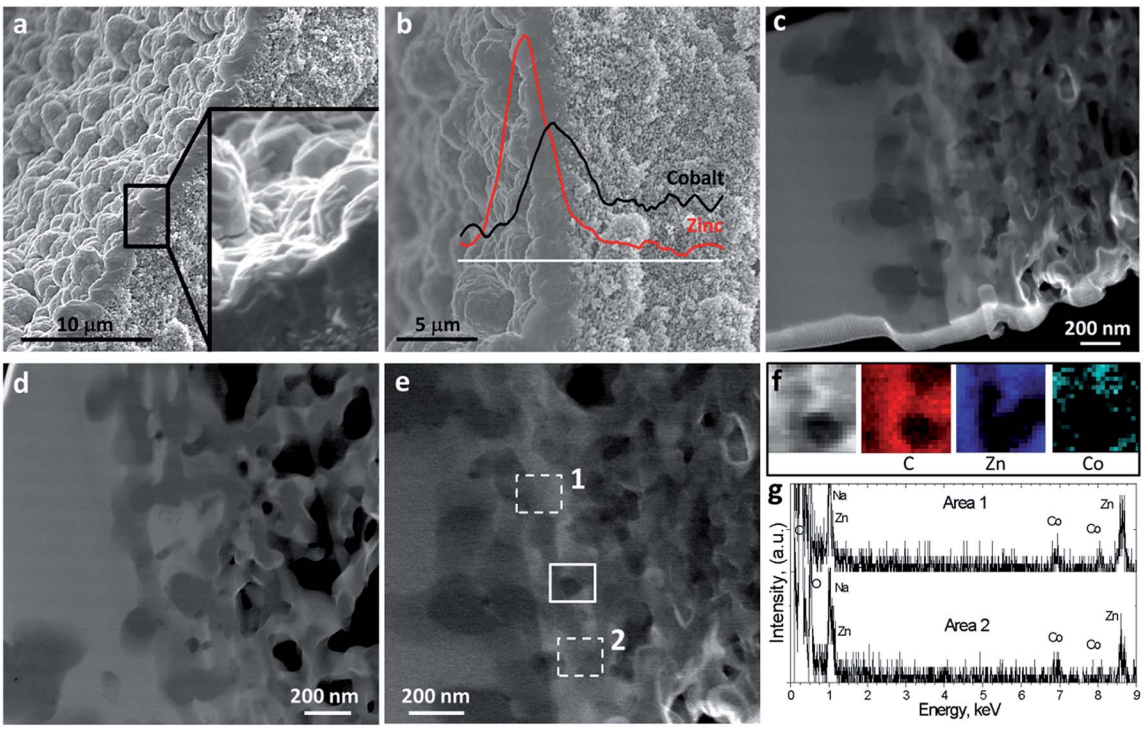

Fig. 3 Electron microscopy analyses of the double-layered ZIF-8/ZIF-9@P84 membrane. HF cross section depicts a 2.0 ± 0.4 μm thick ZIF layer together with a 3-fold magnification inset showing polyhedral ZIF crystals (a). The presence of outer-Zn from ZIF-8 and inner-Co from ZIF-9 coming from the stepwise microfluidic synthesis was confirmed by EDS (b). A wide MOF–support interphase was observed by STEM-HAADF in the lamella extracted by FIB, showing a strong ZIF–polymer interpenetration (c). HAADF Z-contrast shows the location of heavy Zn and Co atoms (lighter contrast) and polymer (dark contrast) (d). STEM-HAADF image magnification of the MOF–polymer interpenetration at a different location in the lamella (e). EDS elemental maps showing the spatial distribution of C, Zn and Co in the area marked with continuous line in (e) and (f). EDS analysis of areas 1 and 2 marked with dashed line in (e) and (g).

analyses confirmed the coexistence of Zn and Co ZIFs at the polymer interface.

The crystalline arrangement of the collected ZIF powders was confirmed by XRD (Fig. 4a). Although both ZIF-9 and ZIF-8 and -67 share the same sod-structure, their XRD patterns were different because they have different crystallographic systems: body-centered cubic for ZIF-8 and -67 and hexagonal for ZIF-9.[55] ZIF-9 showed its typical as-synthesized XRD pattern with traces of its narrow pore phase.[37,65] Fig. 4a shows the XRD spectrum of the double-layered ZIF@P84 HF membranes, scarcely displaying crystalline diffraction coming from the outermost ZIF-8 in addition to the amorphous polymer spectrum. Peaks from ZIF-9, in a thin layer sandwiched between polymer and ZIF-8, were not observed. FTIR spectra of the powder collected through the double-layered ZIF-67/ZIF-9 HF membrane showed the presence of both mIm (from ZIF-67) and bIm (from ZIF-9) imidazolate ligands together with the band at 428 cm^{-1} corresponding to Co–N bonding (Fig. 4b).

The permeation properties of the single and double layered membranes obtained at two different temperatures are shown in Table 1 and Fig. 5. Both ZIF-67 and ZIF-8 materials coating a ZIF-9 supported on P84 hollow fibers provided an improvement in the H_2/CO_2 separation selectivity at both temperatures (35 and 150 °C) with respect to the performance of the single-layer membranes. A decrease in the CO_2 permeances was always observed in the double-layered membranes. This is related to an inhibited CO_2 adsorption on the mIm-ZIF but also with a less defective ZIF double layer inside the HF, giving rise to an increase in the CO_2 retention due to its larger kinetic diameter as compared to H_2 (Fig. 5). Fig. S6 in the ESI† provides an additional individual comparison between the single and double-layered membranes and highlights the positive influence of the double layer in the membrane performance, in agreement with the previous molecular simulation predictions.

Single-layer ZIF-8@P84H_2 permeance at 35 °C was in agreement with our previous work (11.8×10^{-9} *versus* 13.1×10^{-9} mol m^{-2} s^{-1} Pa^{-1}, respectively)[50] where the ZIF-8 layer was 1.3 μm thick. A 1.1 ± 0.1 μm layer was observed by SEM in a pure ZIF-9@P84 membrane, which provided a slightly higher H_2 permeance (14.1×10^{-9} mol m^{-2} s^{-1} Pa^{-1}). The stepwise ZIF-8 growth applied on the ZIF-9 layer then increased the overall thickness about 0.9 μm (resulting in a 2.0 μm double-layer, see Fig. 3a). This may include the interpenetration zone between both ZIFs above mentioned. With similar synthesis procedures but using a polysulfone HF support, the ZIF-9 (ZIF-7 in that case) layer also turned out to be thinner than that of ZIF-8 (*i.e.* 2.4 *vs.* 3.6 μm).[7] It is worth mentioning that a pure ZIF-67@P84 membrane (with a layer thickness of 1.2 ± 0.1 μm, as observed by SEM), not included in Table 1, provided a low quality membrane with the lowest H_2/CO_2 selectivity of 3.6 and a 10.8 ×

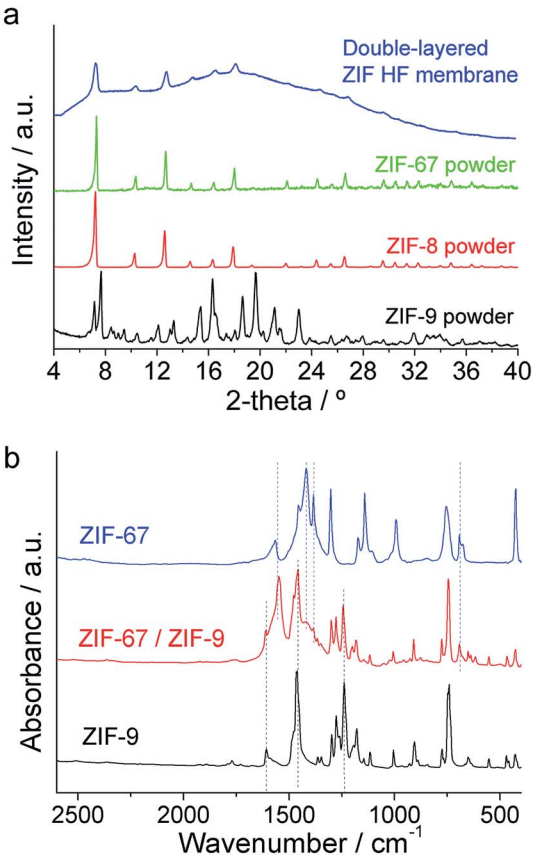

Fig. 4 XRD (a) and FTIR (b) spectra of the ZIF powders collected during the microfluidic syntheses. ZIF-8 with Zn and the Co-based ZIF-67 and ZIF-9 crystallize with the sod-structure. XRD spectrum of the double-layered ZIF@P84 HF membranes is also shown.

10^{-9} mol m^{-2} s^{-1} Pa^{-1} H_2 permeance. However, this did not impede the role (similarly to that of ZIF-8) of ZIF-67 in the CO_2 adsorption inhibition in a double-layered membrane.

Regarding the double-layered membranes, a lower H_2 permeance (9.9×10^{-9} *versus* 12.2×10^{-9} mol m^{-2} s^{-1} Pa^{-1} at 35 °C, respectively) was obtained with the ZIF-67/ZIF-9@P84 with respect to the ZIF-8/ZIF-9@P84 membrane. This is in agreement with the lower permeance obtained with the pure ZIF-67@P84 membrane than with the pure ZIF-8@P84 together with a slightly narrower limiting pore diameter of the ZIF-67 as compared to ZIF-8 (Table S1†).[66] At the same time, an even

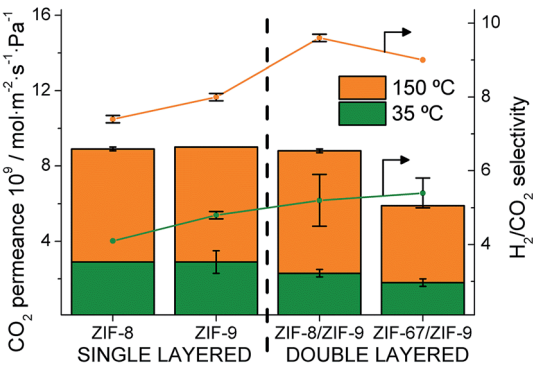

Fig. 5 CO_2 permeance and H_2/CO_2 separation selectivity for single and double-layered ZIF@P84 membranes at 35 °C (green) and 150 °C (orange).

higher permeance was observed with the ZIF-8/ZIF-9 double-layer membrane as compared with a pure ZIF-8 membrane (12.2×10^{-9} *versus* 11.8×10^{-9} mol m^{-2} s^{-1} Pa^{-1} at 35 °C, respectively). This can be related to a thicker ZIF-8 layer coming from direct growth on the rough surface of the pure polymer instead of on the smoother ZIF-9 layer surface, as shown above.

At 150 °C, a 9.6 selectivity and an 83.9×10^{-9} mol m^{-2} s^{-1} Pa^{-1} H_2 permeance (250 GPU, gas permeation unit) were measured with a ZIF-8/ZIF-9@P84 membrane (9.0 selectivity and 53.3×10^{-9} mol m^{-2} s^{-1} Pa^{-1} H_2 permeance, 159 GPU, for the ZIF-67/ZIF-9@P84 membrane). At 35 °C, a slight increase in the selectivity was observed: 5.2 and 5.4 (after growing ZIF-8 and ZIF-67, respectively) instead of 4.8 with single ZIF-9 suggesting a diminished CO_2 adsorption and hence a less-competitive H_2 permeation in comparison with a pure ZIF-9 HF-supported membrane. Meanwhile, the pure ZIF-8 and ZIF-67 membranes had a poor effect on the H_2/CO_2 separation (a selectivity of 3.6 and 4.1, respectively, were obtained at 35 °C, below the Knudsen value for the mixture, 4.9).[27,28]

High temperatures led to a lower CO_2 adsorption and therefore a higher free microporous volume through which the H_2 could diffuse to a large extent, resulting in an enhancement of both H_2 permeance and selectivity.[67,68] The XRD spectra of the ZIF powdered materials after a 175 °C treatment for 24 h are shown in Fig. S7,† accounting for the MOF stability when subjected to the testing conditions. Fig. 6 shows an increasing trend for permeances and selectivities in the 35–150 °C range

Table 1 Permeation properties of the single and double-layered ZIF membranes fabricated inside P84 HF supports in the pre-combustion H_2/CO_2 mixture separation. Permeances and separation selectivities at 35 and 150 °C are shown, together with the 99% confidence intervals of each measure. Pure ZIF-9@P84 membrane values were averaged from two different membranes

	H_2 permeance at 35 °C			H_2 permeance at 150 °C		
	mol m^{-2} s^{-1} Pa^{-1}	GPU	α_{H_2/CO_2}	mol m^{-2} s^{-1} Pa^{-1}	GPU	α_{H_2/CO_2}
ZIF-8/ZIF-9@P84	$12.2 \pm 2.4 \times 10^{-9}$	36	5.2 ± 0.7	$83.9 \pm 0.4 \times 10^{-9}$	250	9.6 ± 0.1
ZIF-67/ZIF-9@P84	$9.9 \pm 0.5 \times 10^{-9}$	29	5.4 ± 0.4	$53.3 \pm 0.2 \times 10^{-9}$	159	9.0 ± 0.0
ZIF-9@P84	$14.1 \pm 3.2 \times 10^{-9}$	42	4.8 ± 0.1	$71.9 \pm 0.2 \times 10^{-9}$	215	8.0 ± 0.1
ZIF-8@P84	$11.8 \pm 0.1 \times 10^{-9}$	35	4.1 ± 0.0	$65.9 \pm 1.1 \times 10^{-9}$	197	7.4 ± 0.1

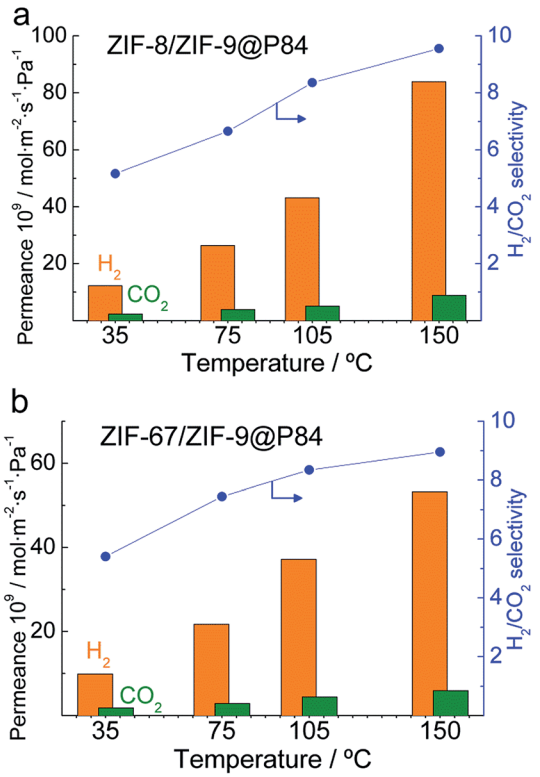

Fig. 6 Double-layered ZIF-8/ZIF-9 (a) and ZIF-67/ZIF-9 (b) membrane permeation properties in the H_2/CO_2 mixture separation as a function of temperature.

for the double-layered ZIF-8/ZIF-9 and ZIF-67/ZIF-9@P84 membranes. Fig. S8 in the ESI† shows the results obtained in the same manner with the single-layered pure ZIF-9 and ZIF-8@P84 membranes. From the Arrhenius plot of the natural logarithm of the permeance as a function of the inverse of temperature, apparent activation energies (E_a) were calculated (Table 2 and Fig. S9†): 8.8 kJ mol^{-1} for CO_2 permeation was obtained in the case of the ZIF-9@P84 membrane, the lowest of the series $E_{a,ZIF\text{-}9} < E_{a,ZIF\text{-}8} < E_{a,ZIF\text{-}67/ZIF\text{-}9} < E_{a,ZIF\text{-}8/ZIF\text{-}9}$. This is consistent with a high CO_2 adsorption in the pure ZIF-9 and with the above-mentioned CO_2 adsorption decrease achieved by means of the double-layered membrane approach. Higher apparent activation energies were also calculated for H_2 permeation with the double-layered membranes (18.1 kJ mol^{-1} and 16.3 kJ mol^{-1} for ZIF-8/ZIF-9 and ZIF-67/ZIF-9@P84, respectively) than with those with a single ZIF layer. The E_a increase can be associated with a reduction in the gas transport through defects and therefore with an improvement in the membrane quality,[69] and not necessarily with differences in the membrane composition.

Table 2 Apparent activation energies calculated from an Arrhenius plot of the natural logarithm of the permeance values as a function of the inverse of temperature in the 35–150 °C range for the single and double-layered ZIF membranes (see Fig. S8)

	E_{a,H_2}/kJ mol^{-1}	E_{a,CO_2}/kJ mol^{-1}
ZIF-8/ZIF-9@P84	18.1	12.2
ZIF-67/ZIF-9@P84	16.3	11.4
ZIF-9@P84	13.7	8.8
ZIF-8@P84	16.2	10.6

It is worth pointing out that the advantageous combination of the properties of two different MOFs has been achieved in recent years by strategies based on crystallizations starting from mixtures of organic linkers at different ratios.[70,71] Thompson *et al.* achieved a tuning of the effective pore size by mixing imidazole-based ligands forming ZIF-8 and ZIF-7, among others.[27,28] Zhang *et al.* fabricated a ZIF-9-67 mixed linker supported membrane with enhanced CO_2 repulsion: a H_2/CO_2 selectivity of 8.9 was obtained.[23] However, an unprecedented strategy has been followed here: a stepwise ZIF growth on the inside of a polymeric hollow fiber. Unlike the case of mixed-linker MOFs, the physical confinement of the material would have a direct influence on the adsorption behaviour because the gas mixture feed is only in contact with the most external layer (ZIF-8), whereas the inner ZIF-9 is protected from surface phenomena (Fig. 1). Our versatile microfluidic experimental approach[7,49] enables consecutive layer-by-layer ZIF growth with an in-depth control of the synthesis parameters.

Nevertheless, the selectivities obtained experimentally fall far short of those expected for MOF materials supposed to be among those with the most restricted pores (ZIF-9 with 3.0 Å, ZIF-8 and ZIF-67 with 3.4 Å). The ZIF structures have revealed an important flexibility in their bonding and therefore they provide higher effective pore diameters than predicted,[27–29] experimentally leading to weaker molecular sieving than expected. Reported results obtained in the H_2/CO_2 separation with MOF (including ZIF) membranes supported on polymeric hollow fibers are shown for comparison in Table S2 of the ESI.† Further data regarding ZIF membranes on all kinds of supports can be found elsewhere.[16,64,72] Structure flexibility should be assumed during the simulations of gas permeation through ZIF-9 to predict the real mechanisms involved in the pre-combustion H_2/CO_2 mixture separation.

4. Conclusions

The information provided by the combination of molecular simulation and adsorption experiments led to the proposal to fabricate double-layered ZIF-8/ZIF-9@P84 and ZIF-67/ZIF-9@P84 hollow fiber supported membranes. Fewer CO_2-adsorptive methylimidazolate-based ZIF-67 and ZIF-8 coatings reduced the CO_2 concentration on the surface of the ZIF-9 layer, thus enhancing the molecular sieving effect of this material and therefore the selectivity in the H_2/CO_2 mixture separation of the entire membrane.

A microfluidic setup was used for the stepwise preparation ZIF-8 or ZIF-67 coatings on ZIF-9@P84 membranes. This gave rise to Zn/Co double-layered ZIF membranes showing an increase in the H_2/CO_2 separation selectivity together with some decrease in the CO_2 permeances at both 35 and 150 °C compared to the single ZIF-9@P84 HF membrane. An increase in the CO_2 permeation apparent activation energies

($E_{a,ZIF\text{-}9} < E_{a,ZIF\text{-}8} < E_{a,ZIF\text{-}67/ZIF\text{-}9} < E_{a,ZIF\text{-}8/ZIF\text{-}9}$), linked with a CO_2 reduced adsorption, was obtained for the double-layered as compared with the single ZIF-9 membrane. In addition, the increases in the H_2 permeation apparent activation energies for the double-layered membranes suggested an enhancement in membrane quality. The membrane characterization carried out by electron microscopy together with FIB and EDS confirmed the existence of the double-layered ZIF membrane, at least in the case of ZIF-8/ZIF-9@P84, with distinguishable domains for Zn and Co containing ZIF phases.

Finally, the improvements achieved in terms of both H_2/CO_2 separation selectivity and H_2 activation energy suggest synergistic coupling of the ZIF pairs studied. We believe that this research paves the way to a new generation of membranes where the features of different MOFs will be combined to enhance the separation performance.

Acknowledgements

Financial support (MAT2013-40556-R) from the Spanish MINECO, the Aragón Government (DGA, T05) and the European Social Fund is gratefully acknowledged. We also acknowledge the use of the Servicio General de Apoyo a la Investigación-SAI (Universidad de Zaragoza). F. C.-B. acknowledges his DGA predoctoral fellowship. V. S. acknowledges the support of the People Program (CIG-Marie Curie Actions, REA grant agreement no. 321642). I. M.-M. thanks the Spanish MINECO for his predoctoral fellowship. The European Research Council through an ERC Grant (ERC2011-StG-279520-RASPA) is also acknowledged. All the microscopy work was done in the Laboratorio de Microscopías Avanzadas at the Instituto de Nanociencia de Aragón (LMA-INA). The authors acknowledge the LMA-INA for offering access to their instruments and expertise.

References

1 M. Z. Jacobson, *Energy Environ. Sci.*, 2009, **2**, 148–173.
2 R. S. Haszeldine, *Science*, 2009, **325**, 1647–1652.
3 R. W. Baker, *Ind. Eng. Chem. Res.*, 2002, **41**, 1393–1411.
4 D. S. Sholl and R. P. Lively, *Nature*, 2016, **532**, 435–437.
5 S. R. Venna and M. A. Carreon, *Chem. Eng. Sci.*, 2015, **124**, 3–19.
6 H. Yin, J. Wang, Z. Xie, J. Yang, J. Bai, J. Lu, Y. Zhang, D. Yin and J. Y. S. Lin, *Chem. Commun.*, 2014, **50**, 3699–3701.
7 F. Cacho-Bailo, S. Catalán-Aguirre, M. Etxeberría-Benavides, O. Karvan, V. Sebastian, C. Téllez and J. Coronas, *J. Membr. Sci.*, 2015, **476**, 277–285.
8 A. J. Brown, J. R. Johnson, M. E. Lydon, W. J. Koros, C. W. Jones and S. Nair, *Angew. Chem., Int. Ed.*, 2012, **51**, 10615–10618.
9 Y. Liu, G. Zeng, Y. Pan and Z. Lai, *J. Membr. Sci.*, 2011, **379**, 46–51.
10 O. Tzialla, C. Veziri, X. Papatryfon, K. G. Beltsios, A. Labropoulos, B. Iliev, G. Adamova, T. J. S. Schubert, M. C. Kroon, M. Francisco, L. F. Zubeir, G. E. Romanos and G. N. Karanikolos, *J. Phys. Chem. C*, 2013, **117**, 18434–18440.
11 Z. Zhao, X. Ma, A. Kasik, Z. Li and Y. S. Lin, *Ind. Eng. Chem. Res.*, 2013, **52**, 1102–1108.
12 M. J. C. Ordoñez, K. J. Balkus, J. P. Ferraris and I. H. Musselman, *J. Membr. Sci.*, 2010, **361**, 28–37.
13 T. Li, Y. Pan, K. V. Peinemann and Z. Lai, *J. Membr. Sci.*, 2013, **425–426**, 235–242.
14 L. Cao, K. Tao, A. Huang, C. Kong and L. Chen, *Chem. Commun.*, 2013, **49**, 8513–8515.
15 S. Japip, K. S. Liao, Y. Xiao and T. S. Chung, *J. Membr. Sci.*, 2016, **497**, 248–258.
16 E. Adatoz, A. K. Avci and S. Keskin, *Sep. Purif. Technol.*, 2015, **152**, 207–237.
17 A. W. Thornton, D. Dubbeldam, M. S. Liu, B. P. Ladewig, A. J. Hill and M. R. Hill, *Energy Environ. Sci.*, 2012, **5**, 7637–7646.
18 T. Yang, G. M. Shi and T. S. Chung, *Adv. Energy Mater.*, 2012, **2**, 1358–1367.
19 Y. S. Li, F. Y. Liang, H. Bux, W. Yang and J. Caro, *J. Membr. Sci.*, 2010, **354**, 48–54.
20 M. He, J. Yao, Q. Liu, Z. Zhong and H. Wang, *Dalton Trans.*, 2013, **42**, 16608–16613.
21 R. Banerjee, A. Phan, B. Wang, C. Knobler, H. Furukawa, M. O'Keeffe and O. M. Yaghi, *Science*, 2008, **319**, 939–943.
22 W. Morris, B. Leung, H. Furukawa, O. K. Yaghi, N. He, H. Hayashi, Y. Houndonougbo, M. Asta, B. B. Laird and O. M. Yaghi, *J. Am. Chem. Soc.*, 2010, **132**, 11006–11008.
23 C. Zhang, Y. Xiao, D. Liu, Q. Yang and C. Zhong, *Chem. Commun.*, 2013, **49**, 600–602.
24 G. Xu, J. Yao, K. Wang, L. He, P. A. Webley, C. Chen and H. Wang, *J. Membr. Sci.*, 2011, **385–386**, 187–193.
25 W. Morris, N. He, K. G. Ray, P. Klonowski, H. Furukawa, I. N. Daniels, Y. A. Houndonougbo, M. Asta, O. M. Yaghi and B. B. Laird, *J. Phys. Chem. C*, 2012, **116**, 24084–24090.
26 E. Atci and S. Keskin, *J. Phys. Chem. C*, 2012, **116**, 15525–15537.
27 J. A. Thompson, C. R. Blad, N. A. Brunelli, M. E. Lydon, R. P. Lively, C. W. Jones and S. Nair, *Chem. Mater.*, 2012, **24**, 1930–1936.
28 J. A. Thompson, J. T. Vaughn, N. A. Brunelli, W. J. Koros, C. W. Jones and S. Nair, *Microporous Mesoporous Mater.*, 2014, **192**, 43–51.
29 E. Haldoupis, S. Nair and D. S. Sholl, *J. Am. Chem. Soc.*, 2010, **132**, 7528–7539.
30 D. Fairen-Jimenez, S. A. Moggach, M. T. Wharmby, P. A. Wright, S. Parsons and T. Düren, *J. Am. Chem. Soc.*, 2011, **133**, 8900–8902.
31 C. Gücüyener, J. van den Bergh, J. Gascon and F. Kapteijn, *J. Am. Chem. Soc.*, 2010, **132**, 17704–17706.
32 N. Liédana, A. Galve, C. Rubio, C. Téllez and J. Coronas, *ACS Appl. Mater. Interfaces*, 2012, **4**, 5016–5021.
33 D. I. Kolokolov, A. G. Stepanov and H. Jobic, *J. Phys. Chem. C*, 2015, **119**, 27512–27520.
34 R. J. Verploegh, S. Nair and D. S. Sholl, *J. Am. Chem. Soc.*, 2015, **137**, 15760–15771.

35 M. R. Ryder, B. Civalleri, T. D. Bennett, S. Henke, S. Rudić, G. Cinque, F. Fernandez-Alonso and J. C. Tan, *Phys. Rev. Lett.*, 2014, **113**, 215502.
36 P. Zhao, T. D. Bennett, N. P. M. Casati, G. I. Lampronti, S. A. Moggach and S. A. T. Redfern, *Dalton Trans.*, 2015, **44**, 4498–4503.
37 P. Zhao, G. I. Lampronti, G. O. Lloyd, E. Suard and S. A. T. Redfern, *J. Mater. Chem. A*, 2014, **2**, 620–623.
38 P. Zhao, G. I. Lampronti, G. O. Lloyd, M. T. Wharmby, S. Facq, A. K. Cheetham and S. A. T. Redfern, *Chem. Mater.*, 2014, **26**, 1767–1769.
39 A. Huang, Y. Chen, N. Wang, Z. Hu, J. Jiang and J. Caro, *Chem. Commun.*, 2012, **48**, 10981–10983.
40 A. S. Huang and J. Caro, *Angew. Chem., Int. Ed.*, 2011, **50**, 4979–4982.
41 N. Wang, Y. Liu, Z. Qiao, L. Diestel, J. Zhou, A. Huang and J. Caro, *J. Mater. Chem. A*, 2015, **3**, 4722–4728.
42 K. Sumida, D. L. Rogow, J. A. Mason, T. M. McDonald, E. D. Bloch, Z. R. Herm, T. H. Bae and J. R. Long, *Chem. Rev.*, 2012, **112**, 724–781.
43 W. Li, G. Zhang, C. Zhang, Q. Meng, Z. Fan and C. Gao, *Chem. Commun.*, 2014, **50**, 3214–3216.
44 W. Li, P. Su, G. Zhang, C. Shen and Q. Meng, *J. Membr. Sci.*, 2015, **495**, 384–391.
45 Y. Peng, Y. Li, Y. Ban, H. Jin, W. Jiao, X. Liu and W. Yang, *Science*, 2014, **346**, 1356–1359.
46 Q. Li, J. Hedlund, J. Sterte, D. Creaser and A. J. Bons, *Microporous Mesoporous Mater.*, 2002, **56**, 291–302.
47 Ó. de la Iglesia, S. Irusta, R. Mallada, M. Menéndez, J. Coronas and J. Santamaría, *Microporous Mesoporous Mater.*, 2006, **93**, 318–324.
48 A. Huang, N. Wang and J. Caro, *Chem. Commun.*, 2012, **48**, 3542–3544.
49 F. Cacho-Bailo, G. Caro, M. Etxeberría-Benavides, O. Karvan, C. Tellez and J. Coronas, *Chem. Commun.*, 2015, **51**, 11283–11285.
50 F. Cacho-Bailo, G. Caro, M. Etxeberria, O. Karvan, C. Tellez and J. Coronas, *RSC Adv.*, 2016, **6**, 5881–5889.
51 D. Dubbeldam, S. Calero, D. E. Ellis and R. Q. Snurr, *Mol. Simul.*, 2016, **42**, 81–101.
52 C. O. Ania, E. García-Pérez, M. Haro, J. J. Gutiérrez-Sevillano, T. Valdés-Solís, J. B. Parra and S. Calero, *J. Phys. Chem. Lett.*, 2012, **3**, 1159–1164.
53 K. S. Deeg, J. J. Gutiérrez-Sevillano, R. Bueno-Pérez, J. B. Parra, C. O. Ania, M. Doblaré and S. Calero, *J. Phys. Chem. C*, 2013, **117**, 14374–14380.
54 A. Garcia-Sanchez, C. O. Ania, J. B. Parra, D. Dubbeldam, T. J. H. Vlugt, R. Krishna and S. Calero, *J. Phys. Chem. C*, 2009, **113**, 8814–8820.
55 K. S. Park, Z. Ni, A. P. Cote, J. Y. Choi, R. D. Huang, F. J. Uribe-Romo, H. K. Chae, M. O'Keeffe and O. M. Yaghi, *Proc. Natl. Acad. Sci. U. S. A.*, 2006, **103**, 10186–10191.
56 B. Zornoza, B. Seoane, J. M. Zamaro, C. Téllez and J. Coronas, *ChemPhysChem*, 2011, **12**, 2781–2785.
57 Y. T. Liao, S. Dutta, C. H. Chien, C. C. Hu, F. K. Shieh, C. H. Lin and K. W. Wu, *J. Inorg. Organomet. Polym. Mater.*, 2015, **25**, 251–258.
58 W. Cai, T. Lee, M. Lee, W. Cho, D. Y. Han, N. Choi, A. C. K. Yip and J. Choi, *J. Am. Chem. Soc.*, 2014, **136**, 7961–7971.
59 S. Aguado, G. Bergeret, M. P. Titus, V. Moizan, C. Nieto-Draghi, N. Bats and D. Farrusseng, *New J. Chem.*, 2011, **35**, 546–550.
60 S. S. Han, S. H. Choi and W. A. Goddard, *J. Phys. Chem. C*, 2010, **114**, 12039–12047.
61 R. Banerjee, H. Furukawa, D. Britt, C. Knobler, M. O'Keeffe and O. M. Yaghi, *J. Am. Chem. Soc.*, 2009, **131**, 3875–3877.
62 X. Wu, J. Huang, W. Cai and M. Jaroniec, *RSC Adv.*, 2014, **4**, 16503–16511.
63 K. Eum, K. C. Jayachandrababu, F. Rashidi, K. Zhang, J. Leisen, S. Graham, R. P. Lively, R. R. Chance, D. S. Sholl, C. W. Jones and S. Nair, *J. Am. Chem. Soc.*, 2015, **137**, 4191–4197.
64 W. Li, Y. Zhang, Q. Li and G. Zhang, *Chem. Eng. Sci.*, 2015, **135**, 232–257.
65 M. He, J. Yao, L. Li, K. Wang, F. Chen and H. Wang, *ChemPlusChem*, 2013, **78**, 1222–1225.
66 P. Krokidas, M. Castier, S. Moncho, D. N. Sredojevic, E. N. Brothers, H. T. Kwon, H. K. Jeong, J. S. Lee and I. G. Economou, *J. Phys. Chem. C*, 2016, **120**, 8116–8124.
67 Q. Liu, N. Wang, J. Caro and A. Huang, *J. Am. Chem. Soc.*, 2013, **135**, 17679–17682.
68 A. Huang, W. Dou and J. Caro, *J. Am. Chem. Soc.*, 2010, **132**, 15562–15564.
69 A. Navajas, R. Mallada, C. Téllez, J. Coronas, M. Menéndez and J. Santamaría, *J. Membr. Sci.*, 2007, **299**, 166–173.
70 A. D. Burrows, *CrystEngComm*, 2011, **13**, 3623–3642.
71 J. Kahr, J. P. S. Mowat, A. M. Z. Slawin, R. E. Morris, D. Fairen-Jimenez and P. A. Wright, *Chem. Commun.*, 2012, **48**, 6690–6692.
72 J. Yao and H. Wang, *Chem. Soc. Rev.*, 2014, **43**, 4470–4493.